Near-field interference map due to a dipolar emission near the edge of a monocrystalline gold platelet

OPEN ACCESS
IOP Publishing
Journal of Optics
J. Opt. **24** (2022) 125001 (6pp)
https://doi.org/10.1088/2040-8986/ac9a5a

Near-field interference map due to a dipolar emission near the edge of a monocrystalline gold platelet

N Abbasirad[1,*], A Barreda[1,2], D Arslan[1,2], M Steinert[1], Y-J Chen[3], J-S Huang[3], I Staude[1,2], F Setzpfandt[1,4] and T Pertsch[1,4]

[1] Institute of Applied Physics, Abbe Center of Photonics, Friedrich Schiller University Jena, Albert-Einstein-Str. 15, 07745 Jena, Germany
[2] Institute for Solid State Physics, Friedrich Schiller University Jena, Helmholtzweg 3, 07743 Jena, Germany
[3] Research Department of Nanooptics, Leibniz Institute of Photonic Technology, Albert-Einstein Str. 9, 07745 Jena, Germany
[4] Fraunhofer Institute of Applied Optics and Precision Engineering, Albert-Einstein-Str. 7, 07745 Jena, Germany

E-mail: najmeh.abbasirad@uni-jena.de

Received 20 June 2022, revised 11 October 2022
Accepted for publication 13 October 2022
Published 31 October 2022

Abstract

Point source excitation and point detection in the near-field provides new perspective to study the near-field optical phenomena of plasmonic nanostructures. Using the automated dual-tip scanning near-field optical microscope (SNOM), we have measured the optical near-field response of a dipolar emission near the edge of a monocrystalline gold platelet. The image dipole method was used to analytically calculate the interference pattern due to surface plasmon polaritons excited at the position of aperture tip and those reflected from edges of the gold platelet. The near-field enhancement was observed on the edges of the gold platelet. Our results verify that automated dual-tip SNOM is an intriguing technique for quantum plasmonic studies where deterministic coupling of quantum emitters and the detection of the near-field enhancement are of great interest.

Keywords: plasmonics, image dipole, surface plasmon polaritons, near-field, aperture SNOM, dual-tip SNOM

(Some figures may appear in colour only in the online journal)

1. Introduction

Plasmonic systems provide unique platforms to manipulate light propagation at subwavelength scales due to excited surface plasmon polaritons (SPPs) at a dielectric/metal interface [1]. However, to fully exploit SPPs for on-chip integration, the absorption losses of plasmonic platforms should be overcome. One of the approaches to reduce scattering losses is to improve the quality of metallic structures by decreasing its roughness. In addition, a particular structural shape and material properties of the structure can be chosen to minimize ohmic losses [2–4]. Monocrystalline gold platelets are a suitable platform for future quantum plasmonics [5, 6]. For instance, a quantum emitter close to the edge of a monocrystalline gold platelet was investigated in the far-field to show the potential of monocrystalline gold platelets as multi input/output platform for quantum plasmonic [7]. However, far-field characterization techniques cannot resolve the SPPs propagation paths on monocrystalline gold platelets. The near-field scanning optical

* Author to whom any correspondence should be addressed.

microscope (SNOM), as a well-established near-field technique has been vastly used to characterize SPPs near-field patterns on the surface of metallic films, such as gold platelets [6, 8, 9]. The two operation modes of aperture SNOM are illumination and collection modes. In the illumination mode, the aperture tip illuminates a sample through a subwavelength aperture. The evanescent waves that pass through the sample or are scattered, are collected with a microscope objective in the far-field. The emitted radiation from an aperture tip near a gold or silver film acts as a point source for the excitation of SPPs. The scattering, reflection, or interference of SPPs due to the structured plasmonic material is manifested in a modified emission pattern [10]. The collection mode is used to image beyond the diffraction limit in the near-field. In the collection-mode SNOM, light is often focused on the sample through an objective, and the aperture tip maps the near-field distribution over a sample. Using the aperture SNOM, SPP modes in plasmonic interfaces, waveguides or nanostructures have been mapped [11–17]. Moreover, scattering SNOM gained its popularity while it can produce near-field images with better spatial resolution than the aperture SNOM [18, 19]. In addition, the scattering SNOM provides direct access to the phase of the field in comparison with the aperture SNOM, where the phase retrieval of the field is not straightforward [20]. However, for both aperture SNOM and scattering SNOM, due to the complex nature of the image formation, a thorough analysis of acquired near-field images remains a very challenging task [21, 22].

A single-tip SNOM has demonstrated its feasibility for analyzing the propagation of SPPs excited at metal-dielectric surfaces and the SPPs propagation and scattering by periodic arrays of surface scatterers at telecom wavelengths [23, 24]. The near-field detection of SPPs using the single-tip SNOM requires far-field illumination. As a result, the diffraction limited far-field illumination obscures the details of the near-field interference pattern due to only SPPs excitation [6, 8, 25–27]. Unlike single-tip SNOM, a dual-tip SNOM allows point-source excitation at the desired position of a sample, eliminating the effect of the far-field illumination on the mapped near-field pattern [28–30]. Hence, dual-tip SNOM is a suitable instrument to investigate SPPs propagation and their interference pattern in the near-field.

The automated dual-tip SNOM has already been used to map the near-field response of a dipolar emission near planar [31] and nanostructured photonic systems [32]. In this work, the dipolar emission from the excitation tip excited SPPs near the edge of a hexagonal gold platelet, while the automated detection tip mapped the corresponding near-field pattern. We have observed both the interference pattern due to the excited SPPs at the excitation tip position with the reflected SPPs from the edge of the goldplatelet, as well as, the SPPs excited along the edge of the gold platelet. We show that the analytical image dipole method is well suited to describe the interference pattern. We demonstrate that the analytical calculation is in excellent agreement with numerical and experimental results. Furthermore, we managed to extract the SPPs wavelength from the near-field interference pattern.

2. Results

2.1. Dipolar emission at an air-metal interface

Figure 1(a) shows an electric dipole $\mathbf{p} = (p_x, p_y, p_z)$, located at distance $z = d$ from an dielectric-gold interface, oscillating with a constant frequency ω which gives rise to an electric field distribution $\mathbf{E}$. The electric field radiated by such a dipole can be written in a cylindrical basis (E_ρ, E_φ, E_z) as, [33, 34]

$$\mathbf{E}_{\mathrm{n}} = 2\Re\left[\frac{\exp(ik_{\mathrm{SPP}}\rho)}{\sqrt{k_{\mathrm{SPP}}\rho}}\exp(ik_{z,n}|z|)\exp(ik_{z,1}|d|)\exp(-i\omega t)\right] \mathrm{M}\vec{v}\left[\mathrm{p}_x\cos\varphi + \mathrm{p}_y\sin\varphi + \mathrm{p}_z(\mathrm{sgn}(d)\frac{k_{\mathrm{SPP}}}{k_{z,1}})\right], \tag{1}$$

where $k_{\mathrm{SPP}} = \frac{2\pi}{\lambda_0}\sqrt{\frac{\epsilon_1\epsilon_2}{\epsilon_1+\epsilon_2}}$ is the propagation constant of SPPs with the radiation wavelength λ_0 in free space. $k_0 = \frac{2\pi}{\lambda_0}$ is the wave vector in vacuum and the dielectric constants of the dielectric and metal correspond to ε_1 and ε_2, respectively. The subscript n can take the values 1 or 2 and refers to the material that contains the dipole (1) and the material on the opposite side of the interface, which does not contain the dipole (2). Constant ${k_{z,n}}^2 = {k_0}^2\epsilon_n - {k_{\mathrm{SPP}}}^2$ indicates the exponential decay of SPPs from an interface into the dielectric or metal depending on the n value. The root is chosen such that $\mathrm{Im}(k_{z,n}) > 0$. The constant $\mathrm{M} = -\frac{1}{2}\left(\frac{k_{z,1}k_{z,2}}{\sqrt{2\pi\epsilon_0}}\right)\left(\frac{k_{z,1}\epsilon_2 - k_{z,2}\epsilon_1}{{\epsilon_1}^2 - {\epsilon_2}^2}\right)e^{(-i\pi/4)}$ is called coupling coefficient [34]. The vector $\vec{v} = \hat{\rho} - \mathrm{sgn}(z)\left(\frac{k_{\mathrm{spp}}}{k_{z,n}}\right)\hat{z}$ denotes the polarization of SPPs waves. The distance of the dipole from the interface d is defined to be positive when the dipole is located above and negative if it is located below the interface on the z-axis.

The angular dependence of SPPs propagation on the xy plane is determined by the angle φ.

A semi-analytical approach based on the image dipole method was proposed to calculate the emission pattern due to excited SPPs by a dipole on planar geometries with edges [35]. In the proposed image dipole method, the SPPs reflected from edges can be substituted by SPPs originating from image dipoles. The positions of the image dipoles are calculated by mirroring the original dipole over all edges. The second-order images are neglected due to the attenuation of the amplitude of the second image dipole induced by the first one.

The proposed image dipole also works for magnetic dipoles and not only for the electric ones. In particular, the field of a magnetic dipole with moment $\mathbf{m}$ can be derived from the field of an electric dipole moment $\boldsymbol{\mu}$ by simply performing the substitution [36]:

$$[\mathbf{E}, \mathbf{H}, \mu_0\mu, \epsilon_0\epsilon, \boldsymbol{\mu}] \rightarrow [\mathbf{H}, -\mathbf{E}, \epsilon_0\epsilon, \mu_0\mu, \mu\mathbf{m}]. \tag{2}$$

Figure 1(b) illustrates an in-plane electric dipole (red arrow) and its image dipoles (green arrows) relative to the edges of a hexagon-like gold platelet. The position of the original dipole corresponds to the aperture position of the

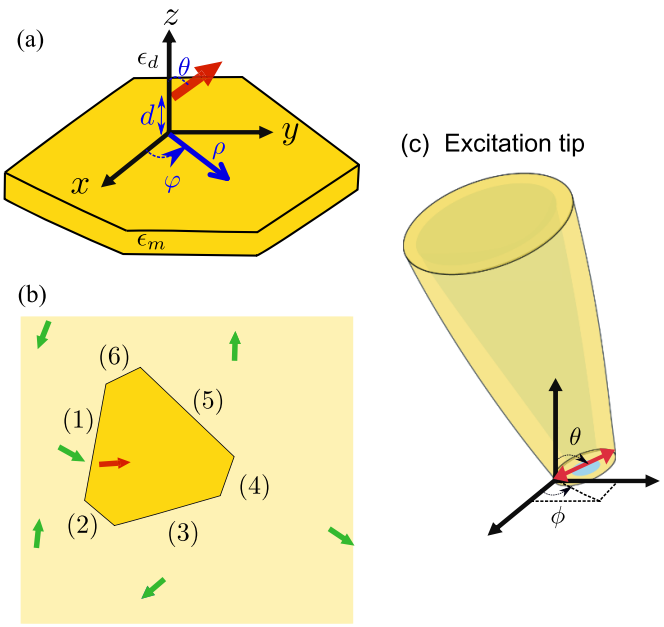

Figure 1. (a) Coordinate of a dipole emission above the gold platelet at a height z = d. The red arrow represents an electric dipole. The radial position of the excited SPPs is ρ and their angular dependence is indicated by φ. (b) Schematic of the dipole image method. The red arrow shows the position of the in-plane original dipole (emission from the excitation tip) and its orientation. The green arrows are the images of the original dipole relative to the gold platelet edges. (c) Angles θ and ϕ of a magnetic dipole representing the dipolar emission from the excitation tip.

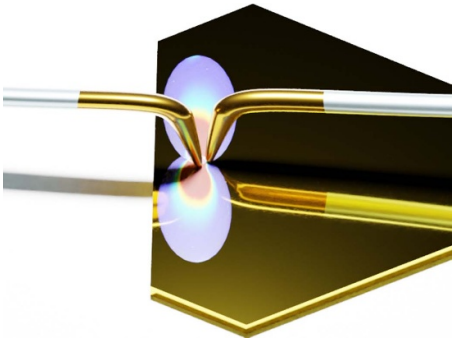

Figure 2. Artistic view of excitation and detection fiber tip on the edge of a gold platelet.

excitation tip of the dual-tip SNOM (figure 2). The edge next to the excitation tip is numbered (1). The electric field intensity distribution on a plane $z = d$ above the air-gold interface is calculated using equation (1). The electric field intensity of SPPs is the result of the interference between the electric field of SPPs generated by the original dipole $\mathbf{p}_0$ and six image dipoles $\mathbf{p}_{1-6}$, is given by,

$$|\mathbf{E}|^2 = C\left|\sum_{n=0}^{6}\frac{\exp(ik_{\mathrm{SPP}}\rho_n)}{\sqrt{k_{\mathrm{SPP}}\rho_n}} \times \left(p_{(\mathrm{x,n})}\cos\varphi_n + p_{(\mathrm{y,n})}\sin\varphi_n + p_{(z,n)}\right)\left(\frac{k_{\mathrm{SPP}}}{k_{z,d}}\right)\right|^2, \quad (3)$$

where $C = |\mathrm{M}\vec{v}\exp(2ik_{z,1}d)\exp(i\omega t)|^2$ and n is the number of the dipoles. $p_{(x,n)}, p_{(y,n)}, p_{(z,n)}$ are the x, y and z components of the image dipoles and can be expressed as, $\mathbf{p}_n = \mathbf{p}_0\Gamma\exp(i\delta)$, Γ being the reflection coefficient of the metal and δ the phase shift between the excited and reflected SPPs. The reflection coefficient and the phase shift should be taken into account since the amplitude and phase of the reflected SPPs change upon the reflection and depend on the dielectric constant of the gold platelet, the surrounding medium, and the incidence angle with which they hit the edges [37]. For normal incidence of the SPPs upon the edges of the gold platelet $\Gamma = 0.15$ and $\delta = 0.35\pi$ [35]. It should be noted that for a gold platelet where the edges are not perpendicular to each other, the incidence angles of SPPs are not always normal. However, it was shown that even for different incidence angles of SPPs, the deviation of the calculated Γ and δ from the values of normal incidence is negligible [38].

2.2. SPPs excitation near the edge of a gold platelet

For the near-field measurements, we have used a gold platelet with thickness of 185 nm with the polycrystalline gold film with a thickness of 220 nm, which acts as the supporting substrate. The excitation tip illuminated the gold platelet about 1 μm away from its edge with a wavelength of $\lambda_0 = 1550$ nm.

An artistic view of the dual-tip SNOM configuration is shown in figure 2. The detection tip automatically maps the near-field pattern of the SPPs around the excitation tip without any collision [31]. The excitation fiber aperture tip acts as a magnetic dipole [39]. Thus, the excited SPPs exhibit the same near-field pattern as if they were excited by a magnetic dipole. When a dipolar emitter excites a gold platelet, its position and radiation wavelength determine which modes are excited and, accordingly, the resulting near-field interference pattern.

Figure 3(a) depicts the mapped SPPs pattern by the detection tip. The SPPs reaching the edges of the gold platelet either reflect or scatter to the free space. The interference of the reflected SPPs from the edges with the excited SPPs at the excitation tip position results in the measured near-field pattern. In particular, we can see that the dipolar emission from the excitation aperture near the edge (1) (see figure 1(b)) leads to the strong intensity along the edge. The edge enhancement of the SPPs was also observed by leakage radiation microscopy [40]. The other edges also show slight enhancement of the near-field intensity, although the SPPs waves decay along the propagation direction. This observation can be attributed to the nanoscale lightening rod effect, i.e. the strong electrical potential gradient due to the small surface curvature at edges [41]. Adjusting the position of the excitation source can be used to alter the near-field pattern and SPPs propagation direction [25].

To gain more insights into the measured near-field pattern, we have compared it with numerical simulations and the semi-analytical model introduced in the previous section. For the simulations, the near-field intensity distribution of the magnetic field, due to a magnetic dipole excitation with azimuthal angle $\phi = 15°$ and polar angle $\theta = 60°$ (figure 1(c)), was calculated on a plane 20 nm above the gold platelet using

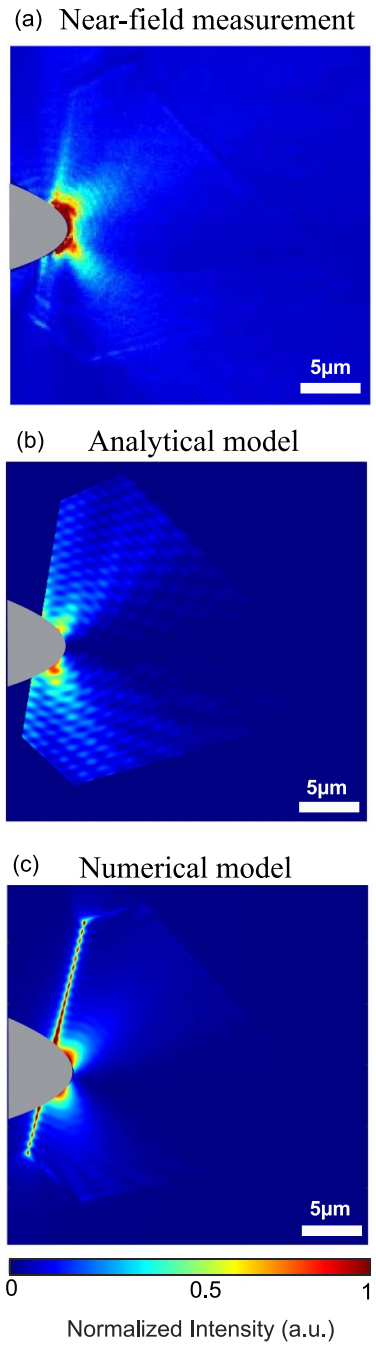

Figure 3. (a) Measured near-field intensity pattern of SPPs due to a dipolar emission from the excitation tip on the edge of a gold platelet. (b) Analytically calculated near-field intensity pattern using the image dipole method. (c) Corresponding numerical simulation of the magnetic field intensity pattern due to a magnetic dipole emission representing the emission from the excitation aperture tip. The gray parabolic regions are the avoidance areas where the intensity information cannot be measured by the detection tip due to the excitation tip geometry. Scale bars denote 5 μm.

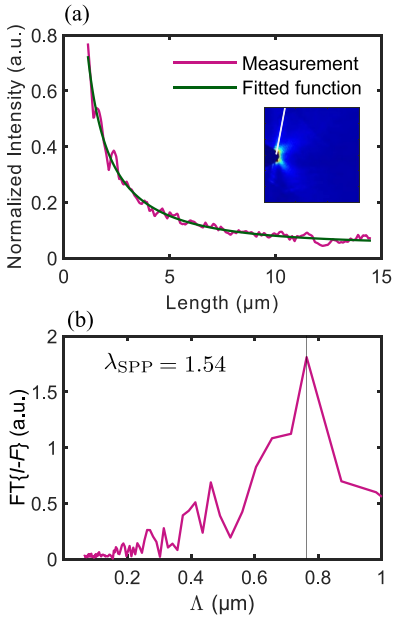

Figure 4. (a) Intensity line profile (I) selected along the white line denoted in the inset of the figure, which corresponds to the near-field measurement in figure 3(a). The intensity line profile was fitted to $\mathrm{F} = \frac{1}{\rho}\exp(-2\mathrm{Im}\{k_{SPP}\}\rho)$. (b) Fourier transform (FT) of the measured intensity line profile (I) in (a) calculated after subtraction from the fitted function ($I - F$). The maximum of the FT corresponds to the half of the wavelength of SPPs that is $\Lambda = 0.77\,\mu$m.

FDTD Solver Lumerical. The angle ϕ of the magnetic dipole in simulations and the electric dipole in the analytical model were chosen based on the orientation of the SPPs propagation in the mapped near-field pattern, whereas the angle θ is defined according to the bent angle of the excitation aperture tip [39]. It must be noted that, due to the duality of electric and magnetic fields near the planar surface, the calculated electric field intensity due the electric dipole excitation shows the similar near-field distribution as a calculated magnetic field intensity due to a magnetic dipole excitation [36]. For that reason, we can compare the numerical results (magnetic field emitted by a magnetic dipole) with the semi-analytical model (electric field emitted by a an electric dipole).

In figure 3(b), the intensity of the analytically calculated electric field shows a very good agreement with the measured near-field intensity in figure 3(a). Figure 3(c) shows the numerically calculated magnetic field intensity. The agreement between the measured near-field, the numerical simulation and the semi-analytical model supports our previous assumptions. This suggest that the image dipole method can substitute the computationally demanding numerical calculation of rather large gold platelet.

Since no far-field illumination is involved, the dual-tip SNOM measurements ensure that the mapped near-field intensity is only the result of the excited SPPs. Therefore, the periodicity of the fringes in the interference pattern should correspond to $\lambda_{SPP}/2$, with λ_{SPP} the wavelength of the excited SPPs. Hence, it is possible to extract the wavelength of the SPPs from the mapped near-field pattern. In doing so, a line where the interferential fringes are clearly observed, is selected in the measured near-field map in figure 3(a). From this line, which is shown in the inset of figure 4(a), we extract the intensity profile along the edge of the gold platelet, starting from the boundary of the avoidance area to the end of

the scan area, as represented in figure 4(a). From the fitting of the intensity line profile to $F = \frac{1}{\rho}\exp(-2\mathrm{Im}\{k_{\mathrm{SPP}}\}\rho)$, SPPs wavelength can be retrieved.

To find the periodicity of the interference fringes corresponding to $\lambda_{\mathrm{SPP}}/2$ and, the fitted exponential function (F) was subtracted from the line intensity profile (I). Then its Fourier transform (FT) was calculated [6]. The reason for subtracting the exponential function from the intensity is to separate two different parts of the signal containing both exponential decay and oscillatory behavior of the SPPs propagation related to the modulation of SPPs standing wave. The peak of the FT is attained at $\Lambda = 0.77$ μm, resulting in the SPPs wavelength $\lambda_{\mathrm{SPP}} = 1.54$ μm. Moreover, from dispersion relation $k_{\mathrm{SPP}} = \frac{2\pi}{\lambda_0}\sqrt{\frac{\epsilon_{\mathrm{d}}\epsilon_{\mathrm{m}}}{\epsilon_{\mathrm{d}}+\epsilon_{\mathrm{m}}}}$ the wavelength of the SPPs at excitation wavelength $\lambda_0 = 1.55$ μm correspond to $\lambda_{\mathrm{SPP}} = 1.54$ μm for the dielectric constant of gold $\epsilon_{\mathrm{m}} = -115.13 + 11.25i$, indicating the excellent agreement with the value extracted from the measurements.

3. Conclusion

In conclusion, it was shown that the dual-tip SNOM allows near-field excitation and detection of SPPs near the edge of plasmonic structures. Since the emission from an excitation aperture tip corresponds to the radiation of a magnetic dipole, the image dipole method can be used to calculate the interference pattern due to the dipole excitation near a planar surface with edges. The SPPs wavelength can be retrieved from the near-field interference pattern measured by the dual-tip SNOM. This works evidenced the unprecedented potential of the automated dual-tip SNOM as a novel characterization technique to study the interference pattern and propagation path of SPPs in plasmonic platforms.

Data availability statement

The data that support the findings of this study are available upon reasonable request from the authors.

Acknowledgments

This work has been funded by the Deutsche Forschungsgemeinschaft (DFG—German Research Foundation) through Collaboration Research Center NOA (Project-ID 39881677-SFB 1375), the international research training group (Project-ID 259607349-GRK2101), the international research training group 2675 'Meta-ACTIVE' (Project Number 437527638), the priority program SPP 1839 Tailored Disorder (Project Number 278747906).

ORCID iDs

N Abbasirad https://orcid.org/0000-0001-9289-6016
A Barreda https://orcid.org/0000-0003-1090-6108
I Staude https://orcid.org/0000-0001-8021-572X

References

[1] Maier S A 2007 *Plasmonics: Fundamentals and Applications* (New York: Springer Science and Business Media)
[2] McPeak K M *et al* 2015 Plasmonic films can easily be better: rules and recipes *ACS Photon.* **2** 326–33
[3] Wu X, Kullock R, Krauss E and Hecht B 2015 Single-crystalline gold microplates grown on substrates by solution-phase synthesis *Cryst. Res. Technol.* **50** 595–602
[4] Krauss E, Kullock R, Wu X, Geisler P, Lundt N, Kamp M and Hecht B 2018 Controlled growth of high-aspect-ratio single-crystalline gold platelets *Cryst. Growth Des.* **18** 1297–302
[5] Huang J-S *et al* 2010 Atomically flat single-crystalline gold nanostructures for plasmonic nanocircuitry *Nat. Commun.* **1** 1–8
[6] Kaltenecker K J *et al* 2020 Mono-crystalline gold platelets: a high-quality platform for surface plasmon polaritons *Nanophotonics* **9** 509–22
[7] Kumar U, Bolisetty S, Mezzenga R, Girard C, Dujardin E and Cuche A 2020 Single plasmon spatial and spectral sorting on a crystalline two-dimensional plasmonic platform *Nanoscale* **12** 13414–20
[8] Walla F, Wiecha M M, Mecklenbeck N, Beldi S, Keilmann F, Thomson M D and Roskos H G 2018 Anisotropic excitation of surface plasmon polaritons on a metal film by a scattering-type scanning near-field microscope with a non-rotationally-symmetric probe tip *Nanophotonics* **7** 269–76
[9] Yao Z, Xu S, Hu D, Chen X, Dai Q and Liu M 2020 Nanoimaging and nanospectroscopy of polaritons with time resolved s-SNOM *Adv. Opt. Mater.* **8** 1901042
[10] Hecht B, Bielefeldt H, Novotny L, Inouye Y and Pohl D W 1996 Local excitation, scattering and interference of surface plasmons *Phys. Rev. Lett.* **77** 1889–92
[11] Weeber J C, Lacroute Y and Dereux A 2003 Optical near-field distributions of surface plasmon waveguide modes *Phys. Rev.* B **68** 115401
[12] Zia R, Schuller J A and Brongersma M L 2006 Near-field characterization of guided polariton propagation and cutoff in surface plasmon waveguides *Phys. Rev.* B **74** 165415
[13] Bouhelier A, Ignatovich F, Bruyant A, Huang C, des Francs G C, Weeber J-C, Dereux A, Wiederrecht G P and Novotny L 2007 Surface plasmon interference excited by tightly focused laser beams *Opt. Lett.* **32** 2535–7
[14] Dvořák P, Neuman T, Břínek L, Šamořil T, Kalousek R, Dub P, Varga P and Šikola T 2013 Control and near-field detection of surface plasmon interference patterns *Nano Lett.* **13** 2558–63
[15] Dvořák P *et al* 2017 Imaging of near-field interference patterns by aperture-type SNOM – influence of illumination wavelength and polarization state *Opt. Express* **25** 16560–73
[16] Matsuura T, Imaeda K, Hasegawa S, Suzuki H and Imura K 2019 Characterization of overlapped plasmon modes in a gold hexagonal plate revealed by three-dimensional near-field optical microscopy *J. Phys. Chem. Lett.* **10** 819–24
[17] Imaeda K, Minoshima W, Tawa K and Imura K 2019 Direct visualization of near-field distributions on a two-dimensional plasmonic chip by scanning near-field optical microscopy *J. Phys. Chem.* C **123** 10529–35
[18] Novotny L, Pohl D W and Hecht B 1995 Scanning near-field optical probe with ultrasmall spot size *Opt. Lett.* **20** 970–2
[19] Bek A, Vogelgesang R and Kern K 2006 Apertureless scanning near field optical microscope with sub-10 nm resolution *Rev. Sci. Instrum.* **77** 043703

[20] Dvořák P, Kvapil M, Bouchal P, Édes Z, Šamořil T, Hrtoň M, Ligmajer F, Křápek V and Šikola T 2018 Near-field digital holography: a tool for plasmon phase imaging *Nanoscale* **10** 21363–8
[21] Schmidt S, Klein A E, Paul T, Gross H, Diziain S, Steinert M, Assafrao A C, Pertsch T, Urbach H P and Rockstuhl C 2016 Image formation properties and inverse imaging problem in aperture based scanning near field optical microscopy *Opt. Express* **24** 4128–42
[22] Neuman T, Alonso-González P, Garcia-Etxarri A, Schnell M, Hillenbrand R and Aizpurua J 2015 Mapping the near fields of plasmonic nanoantennas by scattering-type scanning near-field optical microscopy *Laser Photon. Rev.* **9** 637–49
[23] Gadalla M N, Chaudhary K, Zgrabik C M, Capasso F and Hu E L 2020 Imaging of surface plasmon polaritons in low-loss highly metallic titanium nitride thin films in visible and infrared regimes *Opt. Express* **28** 14536–46
[24] Marquart C, Bozhevolnyi S I and Leosson K 2005 Near-field imaging of surface plasmon-polariton guiding in band gap structures at telecom wavelengths *Opt. Express* **13** 3303–9
[25] Luo S, Yang H, Yang Y, Zhao D, Chen X, Qiu M and Li Q 2015 Controlling wave-vector of propagating surface plasmon polaritons on single-crystalline gold nanoplates *Sci. Rep.* **5** 1–8
[26] Zhang T, Wang C, Chen H, Zhang C, Zhang Z, Fang Y and Zheng H 2019 Controlled multichannel surface plasmon polaritons transmission on atomic smooth silver triangular waveguide *Adv. Opt. Mater.* **7** 1900930
[27] Cao S, Zapata-Herrera M, Campos A, Le Moal E, Marguet S, Dujardin G, Kociak M, Aizpurua J, Borisov A G and Boer-Duchemin E 2020 Probing the radiative electromagnetic local density of states in nanostructures with a scanning tunneling microscope *ACS Photon.* **7** 1280–9
[28] Dallapiccola R, Dubois C, Gopinath A, Stellacci F and Dal Negro L 2009 Near-field excitation and near-field detection of propagating surface plasmon polaritons on au waveguide structures *Appl. Phys. Lett.* **94** 243118
[29] Ren X, Liu A, Zou C, Wang L, Cai Y, Sun F, Guo G and Guo G 2011 Interference of surface plasmon polaritons from a "point" source *Appl. Phys. Lett.* **98** 201113
[30] Fujimoto R, Kaneta A, Okamoto K, Funato M and Kawakami Y 2012 Interference of the surface plasmon polaritons with an Ag waveguide probed by dual-probe scanning near-field optical microscopy *Appl. Surf. Sci.* **258** 7372–6
[31] Abbasirad N, Berzins J, Kollin K, Saravi S, Janunts N, Setzpfandt F and Pertsch T 2019 A fully automated dual-tip scanning near-field optical microscope for localized optical excitation and detection in the visible and near-infrared *Rev. Sci. Instrum.* **90** 053705
[32] Abbasirad N, Barreda A, Arslan D, Steinert M, Fasold S, Rockstuhl C, Staude I, Setzpfandt F and Pertsch T 2021 Investigation of dipole emission near a dielectric metasurface using a dual-tip scanning near-field optical microscope *Nanophotonics* **10** 4511–22
[33] Archambault A, Teperik T V, Marquier F and Greffet J J 2009 Surface Plasmon Fourier optics *Phys. Rev.* B **79** 195414
[34] Mueller J B and Capasso F 2013 Asymmetric surface plasmon polariton emission by a dipole emitter near a metal surface *Phys. Rev.* B **88** 121410
[35] Zhu D, Dong Z, Chu H S, Akimov Y A and Yang J K 2014 Image dipole method for the beaming of plasmons from point sources *ACS Photon.* **1** 1307–12
[36] Novotny L and Hecht B 2012 *Principles of Nano-Optics* (Cambridge: Cambridge University Press)
[37] Gordon R 2006 Vectorial method for calculating the Fresnel reflection of surface plasmon polaritons *Phys. Rev.* B **74** 153417
[38] Zhu D, Dong Z, Chu H S, Akimov Y A and Yang J K W 2014 Image dipole method for the beaming of plasmons from point sources *ACS Photon.* **1** 1307–12
[39] Klein A E, Janunts N, Steinert M, Tünnermann A and Pertsch T 2014 Polarization-resolved near-field mapping of plasmonic aperture emission by a dual-SNOM system *Nano Lett.* **14** 5010–15
[40] Berthelot J, Bouhelier A, Des Francs G C, Weeber J-C and Dereux A 2011 Excitation of a one-dimensional evanescent wave by conical edge diffraction of surface plasmon *Opt. Express* **19** 5303–12
[41] Urbieta M, Barbry M, Zhang Y, Koval P, Sánchez-Portal D, Zabala N and Aizpurua J 2018 Atomic-scale lightning rod effect in plasmonic picocavities: a classical view to a quantum effect *ACS Nano* **12** 585–95